Cu(0) Nanoclusters Derived from Poly(propylene imine) Dendrimer Complexes of Cu(II)

Pierre N. Floriano,[†] Charles O. Noble, IV,[†] J. Michael Schoonmaker,[‡] E. D. Poliakoff,[†] and Robin L. McCarley*,[†]

Contribution from the Choppin Laboratories of Chemistry, Louisiana State University, Baton Rouge, Louisiana 70803-1804, and Center for Advanced Microstructures and Devices, Louisiana State University, 6980 Jefferson Highway, Baton Rouge, Louisiana 70806

Received February 28, 2001

Abstract: A family of diaminobutane core, poly(propylene imine) dendrimers coordinated to Cu(II), DAB-Am_n-$Cu(II)_x$ ($n = 4, 8, 16, 32, 64$, $x = n/2$), was studied by means of extended X-ray absorption fine structure (EXAFS) and X-ray absorption near-edge structure (XANES) spectroscopies. The geometry of the dipropylene triamine (dpt)-Cu(II) end-group complexes for all dendrimer generations is reported for the first time and is found to be that of a square-based pyramid with each Cu ion bound to three nitrogen atoms (Cu−N distance ∼2.03 Å) of the dpt end group of the dendrimer. An oxygen atom residing 1.96 Å from the Cu ion also occupies the equatorial plane, and the pyramid is completed by an axial oxygen at ∼2.65 Å. In addition, we report for the first time that reduction of the Cu(II)-dendrimer complexes with $NaBH_4$ yields DAB-Am_n-$Cu(0)_{cluster}$ species. Transmission electron microscopy (TEM) studies of the reduced species demonstrate that there is a systematic decrease in the size of the generated Cu clusters with increasing dendrimer generation. Additionally, it was found that the size of the nanoclusters is a function of the n/x ratio of the DAB-Am_n-$Cu(II)_x$ precursor, with highly monodisperse, extremely small nanoclusters ($r_{cluster} = 8.0 \pm 1.6$ Å) obtained with $n = 64$ and $x = 16$. EXAFS and XANES measurements on the reduced DAB-Am_n-$Cu(0)_{cluster}$ corroborate the TEM data, and provide additional information on the possible encapsulation of the Cu nanoclusters by the dendrimers.

Introduction

In the past decade, dendritic molecules have caught the attention of a number of researchers due to their outstanding properties that make them suitable for a broad range of applications.[1−3] Dendrimers can serve not only as contrast agents in magnetic resonance imaging[4] and as drug delivery systems in medicine,[5,6] but are expected to contribute significantly in the fields of catalysis,[7,8] molecular recognition,[3] light harvesting,[9] and environmental studies[10] to name a few.

Poly(amidoamine), PAMAM, and poly(propylene imine)-diaminobutane core, DAB, dendrimers, as well as other dendrimers, have been shown to form complexes with metal ions.[11−26] Except for the case of DAB dendrimers,[25,26] it has been shown that such metal-ion-dendrimer precursor species can be used to produce metal nanoparticles upon reduction of the dendrimer-metal complexes.[11−14,16,19,20,22,24] Although a large number of studies have focused on making metal nanoparticles from metal-PAMAM complexes (Au,[11−14] Ag,[11,13] Cu,[16,19,20

* Author to whom correspondence should be addressed. Phone: (225) 578-3239. Fax: (225) 578-3458. E-mail: tunnel@lsu.edu.

[†] Choppin Laboratories of Chemistry, Louisiana State University.

[‡] Center for Advanced Microstructures and Devices, Louisiana State University.

(1) Bosman, A. W.; Janssen, H. M.; Meijer, E. W. *Chem. Rev.* **1999**, *99*, 1665−1688.

(2) Tomalia, D. A.; Hurst, H. D. *Top. Curr. Chem.* **1993**, *165*, 193−313.

(3) Zeng, F.; Zimmerman, S. C. *Chem. Rev.* **1997**, *97*, 1681−1712.

(4) Fischer, M.; Vögtle, F. *Angew. Chem., Int. Ed. Engl.* **1999**, *38*, 885−905.

(5) Liu, M.; Kono, K.; Fréchet, J. M. J. *J. Controlled Release* **2000**, *65*, 121−131.

(6) Freemantle, M. *Chem. Eng. News* **1999**, *November 1*, 27−35.

(7) Reetz, M. T.; Lohmer, G.; Schwickardi, R. *Angew. Chem., Int. Ed. Engl.* **1997**, *36*, 1526−1529.

(8) Knapen, J. W. J.; van der Made, A. W.; de Wilde, J. C.; van Leeuwen, P. W. N. M.; Wijkens, P.; Grove, D. M.; van Koten, G. *Nature* **1994**, *372*, 659−663.

(9) Balzani, V.; Campagna, S.; Denti, G.; Juris, A.; Serroni, S.; Venturi, M. *Acc. Chem. Res.* **1998**, *31*, 26−34.

(10) Kovvali, A. S.; Chen, H.; Sirkar, K. K. *J. Am. Chem. Soc.* **2000**, *122*, 7594−7595.

(11) Balogh, L.; Valluzi, R.; Laverdure, K. S.; Gido, S. P.; Hagnauer, G. L.; Tomalia, D. A. *J. Nanopart. Res.* **1999**, *1*, 353−368.

(12) Grohn, F.; Bauer, B. J.; Akpalu, Y. A.; Jackson, C. L.; Amis, E. J. *Macromolecules* **2000**, *33*, 6042−6050.

(13) Esumi, K.; Suzuki, A.; Yamahira, A.; Torigoe, K. *Langmuir* **2000**, *16*, 2604−2608.

(14) He, J.-A.; Valluzzi, R.; Yang, K.; Dolukhanyan, T.; Sung, C.; Kumar, J.; Tripathy, S. K. *Chem. Mater.* **1999**, *11*, 3268−3274.

(15) Diallo, M. S.; Balogh, L.; Shafagati, A.; Johnson, J. H.; Goddard, W. A., III; Tomalia, D. A. *Environ. Sci. Technol.* **1999**, *33*, 820−824.

(16) Zhao, M.; Crooks, R. M. *Chem. Mater.* **1999**, *11*, 3379−3385.

(17) Ottaviani, M. F.; Bossmann, S.; Turro, N. J.; Tomalia, D. A. *J. Am. Chem. Soc.* **1994**, *116*, 661−671.

(18) Ottaviani, M. F.; Montalti, F.; Turro, N. J.; Tomalia, D. A. *J. Phys. Chem. B* **1997**, *101*, 158−166.

(19) Zhao, M. Q.; Sun, L.; Crooks, R. M. *J. Am. Chem. Soc.* **1998**, *120*, 4877−4878.

(20) Balogh, L.; Tomalia, D. A. *J. Am. Chem. Soc.* **1998**, *120*, 7355−7356.

(21) Liao, Y.-H.; Moss, J. R. *Organometallics* **1996**, *15*, 4307−4316.

(22) Zhao, M.; Crooks, R. M. *Angew. Chem., Int. Ed. Engl.* **1999**, *38*, 364−366.

(23) Bardaji, M.; Kustos, M.; Caminade, A.-M.; Majoral, J.-P.; Chaudret, B. *Organometallics* **1997**, *16*, 403−410.

(24) Chechik, V.; Crooks, R. M. *J. Am. Chem. Soc.* **2000**, *122*, 1243−1244.

(25) Bosman, A. W.; Schenning, A. P. H. J.; Janssen, R. A. J.; Meijer, E. W. *Chem. Ber./Recl.* **1997**, *130*, 725−728.

(26) Vassilev, K.; Ford, W. T. *J. Polym. Sci. Part A.* **1999**, *37*, 2727−2736.

10.1021/ja010549d CCC: $20.00
Published on Web 10/09/2001

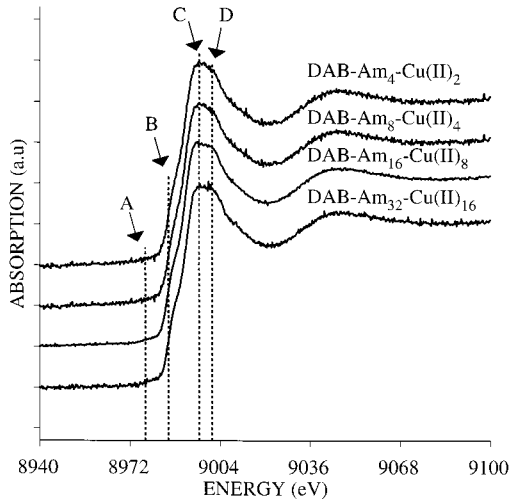

Figure 1. Normalized Cu K-edge XANES spectra for DAB-Am_n-$Cu(II)_x$ (n = 4 to 32, $x = n/2$) complexes in CH_3OH solution.

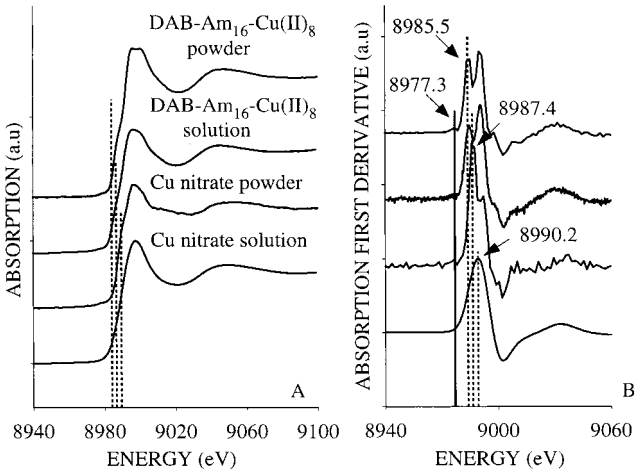

Figure 2. (A) Comparison of the normalized Cu K-edge spectra for DAB-Am_{16}-$Cu(II)_8$ and $Cu(NO_3)_2$ (solid state and solution). (B) Derivative of the corresponding XANES spectra. The dashed lines point at the position of Feature B in Figure 1 and the solid line points at the position of Feature A.

Pd,[22,24] and Pt[22]), we know of no reports focusing on the use of metal-DAB dendrimer complexes for the fabrication of metal nanoclusters.

DAB dendrimers have been shown to form well-defined, stoichiometric complexes with ionic Cu, Zn, Ni, and Co,[25,26] an attribute that may allow for control over the properties of metal nanoclusters derived from such metal-ion-dendrimer complexes. To this end, it would be of great importance to have the ability to obtain structural information for the metal ion complexed in the dendrimer, as well as information regarding the nature of the dendrimer-metal nanoparticle structure following reduction of the metal-ion-dendrimer complex.

We report here, for the first time, an investigation of Cu(II)-poly(propylene imine) dendrimer complexes with a diaminobutane core (DAB-Am_n-$Cu(II)_x$, n = 4 to 64, $x = n/2$) by means of extended X-ray absorption fine structure (EXAFS) and X-ray absorption near-edge structure (XANES) spectroscopies. By studying the EXAFS and XANES spectra of DAB-Am_n-$Cu(II)_x$ at the copper K-edge, we have been able to determine the geometry of the dendrimer end-group complex about the Cu ion and parameters such as bond distances, coordination numbers, and nature of the ligands contributing to the copper coordination sphere. In addition, we have studied the properties of the Cu(0) nanoclusters that result upon reduction of the DAB-Am_n-$Cu(II)_x$ template precursors. The size of the Cu(0) nanoclusters is determined from TEM data, and EXAFS measurements are used to understand the local environment of the reduced Cu nanoclusters. The EXAFS data are useful for correlating the present data with the outcomes from previous studies of nanoparticles.[27−29] The TEM and EXAFS studies demonstrate that the size of the Cu(0) nanoclusters decreases with increased generation of the dendrimer.

Results and Discussion

DAB-Am_n-$Cu(II)_x$ Complexes: Generation-Independent, Square-Based Pyramid Structure. (a) Solution Studies. Normalized, solution-phase, fluorescence mode XANES spectra at the Cu K-edge for the DAB-Am_n-$Cu(II)_x$ complexes (n = 4, 8, 16, 32, $x = n/2$) are displayed in Figure 1. The XANES spectra in Figure 1 support the claim that Cu(II) is the only copper species present, as is demonstrated by the presence of only the expected three major bands for Cu(II).[30−35] In addition, the positions of the spectral features indicate that Cu(II) is bound to nitrogen atoms. Feature B in Figure 1 is known to be associated with a copper 1s → 4p transition with simultaneous shakedown[30,31] and is apparent in the first derivative spectra, as shown in Figure 2B for DAB-Am_{16}−$Cu(II)_8$. The 1s → 4p transition occurs at 8985.5 eV for the entire DAB-Am_n-$Cu(II)_x$ complex series (data not shown), which is typical of Cu(II) complexes.[32] The spectra in Figures 1 and 2 point to the lack of any uncoordinated Cu(II), as observed upon comparison of the spectra for the DAB-Am_n-$Cu(II)_x$ complexes with those of $Cu(NO_3)_2$.[32,35−44] In addition, features C and D further support the +2 oxidation state of copper in the complexes. The 8996.4 eV value for the transition associated with feature C is routinely observed in the XANES spectra of Cu(II)-ligand complexes containing Cu−N bonds and has been described to be caused by a larger degree of covalency between the Cu(II) and equatorial ligands.[32] In addition, feature D is observed at 9001

(27) Montano, P. A.; Shenoy, G. K.; Alp, E. E.; Shulze, W.; Urban, J. *Phys. Rev. Lett.* **1986**, *56*, 2076−2079.
(28) Apai, G.; Hamilton, J. F.; Stöhr, J.; Thompson, A. *Phys. Rev. Lett.* **1979**, *43*, 165−169.
(29) Borowski, M. *J. Phys. IV* **1997**, *C2*, 259−260.
(30) Grunes, L. A. *Phys. Rev. B* **1983**, *27*, 2111−2131.
(31) Bair, R. A.; Goddard, A., III *Phys. Rev. B* **1980**, *22*, 2767−2776.
(32) Kau, L.-S.; Hodgson, K. O.; Solomon, E. I. *J. Am. Chem. Soc.* **1989**, *111*, 7103−7109.
(33) Kau, L.-S.; Spira-Solomon, D. J.; Penner-Hahn, J. E.; Hodgson, K. O.; Solomon, E. I. *J. Am. Chem. Soc.* **1987**, *109*, 6433−6442.
(34) Brown, J. M.; Powers, L.; Kincaid, B.; Larrabee, J. A.; Spiro, T. G. *J. Am. Chem. Soc.* **1980**, *102*, 4210−4216.
(35) Nomura, M.; Kazusaka, A.; Kakuta, N.; Ukisu, Y.; Miyahara, K. *J. Chem. Soc., Faraday Trans. 1* **1987**, *83*, 1227−1235.
(36) A notable difference in the absorption spectra of copper nitrate in solution and in the solid state is observed. This is most likely due to the effect of the MeOH solvent, for the Cu(II) complex may extend its geometry to that of a strongly favored octahedron by weakly binding to solvent molecules or nitrate groups.
(37) Onori, G.; Santucci, A.; Scafati, A.; Belli, M.; Della Longa, S.; Bianconi, A.; Palladino, L. *Chem. Phys. Lett.* **1988**, *149*, 289−294.
(38) Ohtaki, H.; Maeda, M. *Bull. Chem. Soc. Jpn.* **1974**, *47*, 2197.
(39) Magini, M. *Inorg. Chem.* **1982**, *21*, 1535.
(40) Kosugi, N.; Kondoh, H.; Tajima, H.; Kuroda, H. *Chem. Phys.* **1989**, *135*, 149−160.
(41) Choy, J.-H.; Kim, D.-K.; Park, J.-C.; Choi, S.-N.; Kim, Y.-J. *Inorg. Chem.* **1997**, *36*, 189−195.
(42) Martens, G.; Rabe, P.; Schwentner, N.; Werner, A. *Phys. Rev. B* **1978**, *17*, 1481−1488.
(43) Lamberti, C.; Bordiga, S.; Salvalaggio, M.; Spoto, G.; Zecchina, A.; Geobaldo, F.; Vlaic, G.; Bellatrecia, M. *J. Phys. Chem. B* **1997**, *101*, 344−360.
(44) Fitts, J. P.; Trainor, T. P.; Grolimund, D.; Bargar, J. R.; Parks, G. A.; Brown, J. G. E. *J. Synchrotron Radiat.* **1999**, *6*, 627−629.

eV for all generations and is typical of nitrogen-bonded Cu(II) ions.[34,35]

A slight increase in the intensity of feature D, in comparison to the other spectral features, is observed when moving from dendrimer generation 1 to 4, Figure 1. We attribute this intensity increase for feature D to an increase in the degree of covalency of the Cu−N bond as a result of a distortion of the copper-dendrimer complex, possibly caused by increased steric crowding of the Cu(II)-dendrimer complexes with increased dendrimer generation. This distortion is further supported by the presence of feature A at 8977.3 eV in the solution and solid-state (Figure 2A) XANES spectra. The position of spectral feature A is consistent with the electric dipole forbidden 1s → 3d transition[45] associated with a variety of distorted Cu(II)-N complexes.[30,32,46,47]

The electronic (UV/vis) spectra of the DAB-Am$_n$-Cu(II)$_x$ complexes in methanol (MeOH) are virtually indistinguishable and consist of a d−d band near 630 nm.[48−50] Observation of this transition is consistent with trigonal bipyramidal and square-based pyramidal geometries for Cu(II) complexes.[25,48] Electron paramagnetic resonance (EPR) data obtained by Bosman[25,49] for DAB-Am$_n$-Cu(II)$_x$ indicate that the latter case is more likely.[51]

(b) Studies of DAB-Am$_n$-Cu(II)$_x$ in the Solid State. X-ray spectroscopy experiments with DAB-Am$_n$-Cu(II)$_x$ solids were undertaken to obtain high-quality (high signal-to-noise ratio) spectra that could be used to accurately determine the structure of the Cu(II)-dendrimer complexes.[52] Free-flowing "baby blue" DAB-Am$_n$-Cu(II)$_x$ powders were obtained for $n = 4-64$ by vacuum evaporation of the MeOH solvent. Representative XANES spectra for all Cu(II)-dendrimer complexes are displayed in Figure 3. In general, the solid-state spectra are almost identical to the solution-phase spectra (cf. solution and powder spectra for $n = 16$ in Figure 2A), with the differences being associated solely with the intensities of features A and D. As discussed above for the solution-phase spectra, features A and D arise when the geometry of Cu(II)-ligand complexes is distorted.[32,46,47] Thus, the Cu(II)-dendrimer complexes in the solid state have a structure with a higher degree of distortion than when in solution, albeit only slightly more distorted. It can be concluded that the Cu oxidation state and overall structure of the DAB-Am$_n$-Cu(II)$_x$ materials around the Cu ions is virtually the same when the Cu-dendrimer complexes are in the solid state or in MeOH solution.

Analysis of the EXAFS data provides a means of determining bond distances and coordination numbers for Cu(II) in the DAB-Am$_n$-Cu(II)$_x$ materials, and can be utilized to identify the nearest neighbors to Cu(II). Previous studies involving comparison of EPR data for DAB-Am$_n$-Cu(II)$_x$ complexes with that for a *N*,*N*,*N*′,*N*′-tetrakis(3-aminopropyl)-1,5-diamino-3-oxapentane di-copper(II) complex suggest that Cu(II) is most likely coordinated

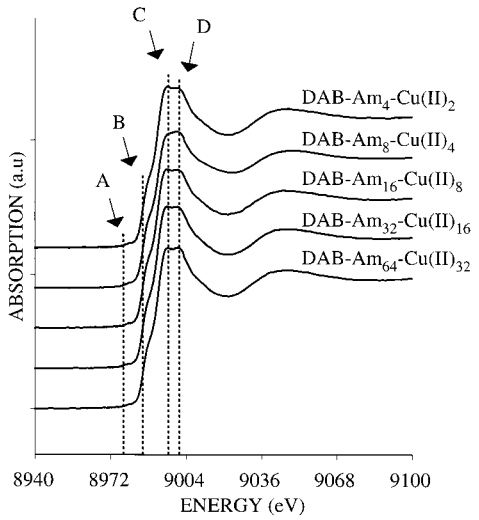

Figure 3. Normalized Cu K-edge XANES spectra for DAB-Am$_n$-Cu(II)$_x$ ($n = 4$ to 64, $x = n/2$) complexes in the solid state.

to two primary amines, one tertiary amine, and two other ligands (such as MeOH or H_2O) in the DAB-Am$_n$-Cu(II)$_x$ complexes.[49,53] Due to the similarity of the atomic weight, size, and electronic configuration of oxygen and nitrogen, their back-scattering functions are sometimes difficult to differentiate and could lead to ambiguities in assignment of ligand identity. However, it is possible to overcome this challenge by comparing the experimental EXAFS data to simulated EXAFS data generated by using all possible combinations of O and N atoms coordinated to Cu(II),[50] comparing the bond distances obtained upon analysis of the EXAFS data to those found for copper−nitrogen and copper−oxygen complexes, *and* evaluation of the back Fourier transforms.

The Fourier transforms of the EXAFS function (experimental-solid lines) and the calculated fits using Feff7[54,55] (dotted lines) are shown in Figure 4 for the five DAB-Am$_n$-Cu(II)$_x$ complexes.[56] Table 1 lists the coordination numbers and bond distances obtained from the curve fitting procedure, as well as the goodness-of-fit parameter, *R*. The shape of the Fourier transform data is reminiscent of that obtained for Cu(II) complexes having one or two axial oxygen ligands;[57−61] the fits of the Fourier transform data and previous literature[41] allow us to clearly identify one axial O atom at about 2.6 Å away from the Cu(II). As determined from the data in Figure 4, the first coordination shell contains a combination of four nitrogen and/or oxygen atoms in the equatorial plane of the complex. But, the Cu-ligand atom bond distances obtained (1.99 Å) are higher than those for known oxygen-coordinated Cu(II) complexes (typical bond distances between 1.85 and 1.96 Å), indicating that the atoms in the equatorial plane are most likely not oxygen but nitrogen.[43]

(45) Sarode, P. R.; Sankar, G.; Rao, C. N. R. *Proc. Indian Acad. Sci. (Chem. Sci.)* **1983**, *92*, 527−542.
(46) Palladino, L.; Della Longa, S.; Reale, A.; Belli, M.; Scafati, A.; Onori, G.; Santucci, A. *J. Chem. Phys.* **1993**, *98*, 2720−2726.
(47) Sano, M.; Komorita, S.; Yamatera, H. *Inorg. Chem.* **1992**, *31*, 459−463.
(48) Lever, A. B. P. *Inorganic Electronic Spectroscopy*, 2nd ed.; Elsevier: Amsterdam, The Netherlands, 1984; Vol. 33.
(49) Bosman, A. W. *Dendrimers in Action*, Ph.D. Dissertation, Technische Universiteit Eindhoven, 1998.
(50) See Supporting Information.
(51) Velayutham, M.; Varghese, B.; Subramanian, S. *Inorg. Chem.* **1998**, *37*, 5983−5991.
(52) Increases in the Cu(II)-dendrimer complex concentration such that X-ray spectra with sufficiently high S/N ratios could be obtained (needed for accurate structural assignments) were met with frustration due to the limited solubility of the Cu(II)-dendrimer complexes in MeOH.
(53) Adams, H.; Bailey, N. A.; Carlisle, W. D.; Fenton, D. E. *Acta Crystallogr.* **1990**, *C46*, 1439−1441.
(54) Rehr, J. J. *Surf. Rev. Lett.* **1995**, *2*, 63−69.
(55) Zabinsky, S. I.; Rehr, J. J.; Ankudinov, A.; Albers, R. C.; Eller, M. J. *Phys. Rev. B* **1995**, *52*, 2995−3009.
(56) http://ixs.csrri.iit.edu.
(57) D'Angelo, P.; Bottari, E.; Festa, M. R.; Nolting, H.-F.; Pavel, N. V. *J. Phys. Chem. B* **1998**, *102*, 3114−3122.
(58) Carrado, K. A.; Wasserman, S. R. *J. Am. Chem. Soc.* **1993**, *115*, 3394−3395.
(59) D'Angelo, P.; Bottari, E.; Festa, M. R.; Nolting, H.-F.; Pavel, N. V. *J. Chem. Phys.* **1997**, *107*, 2807−2812.
(60) Korshin, G. V.; Frenkel, A. I.; Stern, E. A. *Environ. Sci. Technol.* **1998**, *32*, 2699−2705.
(61) Inada, Y.; Ozutsumi, K.; Funahashi, S.; Soyama, S.; Kawashima, T.; Tanaka, M. *Inorg. Chem.* **1993**, *32*, 2.

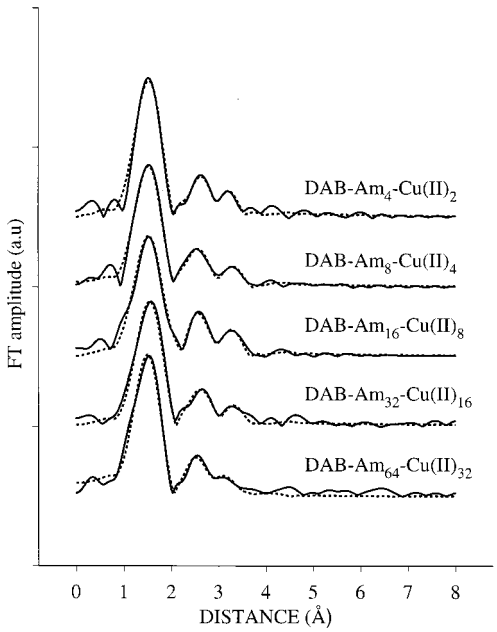

Figure 4. Fourier transforms of the EXAFS function for the DAB-Am_n-$Cu(II)_x$ (n = 4 to 64, $x = n/2$) complexes in the solid state. Experimental data (solid line) and calculated fits (dashed line) are shown. A k range of 3−13 $Å^{-1}$ was used for all of the Fourier transforms so as to eliminate low- and high-k noise contributions.

Table 1. EXAFS Parameters Obtained from Curve Fitting Analysis for the DAB-Am_n-$Cu(II)_x$ (n = 4 to 64, $x = n/2$) Complexes

sample	element	coord. no.[a]	bond dist. (Å)[b]	Debye−Waller factor (σ^2)[a]	R
DAB-Am_4-$Cu(II)_2$	N, O	4	1.99	0.0071	15
	O	1	2.67	0.0118	
	C	3	3.03	0.0062	
	Cu	1	3.36	0.0078	
DAB-Am_8-−$Cu(II)_4$	N, O	4	2.00	0.0089	10
	O	1	2.64	0.0125	
	C	3	3.00	0.0065	
	Cu	1	3.50	0.0107	
DAB-Am_{16}-$Cu(II)_8$	N, O	4	1.99	0.0089	12
	O	1	2.60	0.0168	
	C	3	2.99	0.0078	
	Cu	1	3.45	0.0082	
DAB-Am_{32}-$Cu(II)_{16}$	N, O	4	2.01	0.0081	15
	O	1	2.68	0.0146	
	C	3	3.03	0.0083	
	Cu	1	3.47	0.0109	
DAB-Am_{64}-$Cu(II)_{32}$	N, O	4	2.00	0.0087	18
	O	1	2.61	0.0104	
	C	3	3.01	0.0067	
	Cu	1	3.42	0.0107	

[a] The generally accepted value for the accuracy of Debye−Waller factors and coordination numbers is ±10%; see footnote *c*. [b] The accuracy on distances is taken as ±0.01 Å; see footnote *c*. [c] Teo, B. K. *EXAFS, Basic Principles and Data Analysis*; Inorganic Chemistry Concepts Series; Springer-Verlag: New York, 1986; Vol. 9.

To identify the ligand atoms in the equatorial plane, the first coordination peak centered at 1.6 Å (without phase-shift correction) in the Fourier transform data that corresponds to the contribution of the four equatorial atoms was back transformed to k space (see Figure 5). Then, the k space data were fitted by using standard procedures.[54,55] The best fit to the experimental data was obtained through the use of a model with 3 nitrogen atoms and 1 oxygen atom in the equatorial plane; all other combinations gave significantly higher R values (Table T-1 of the Supporting Information).[62,63] Similar results were

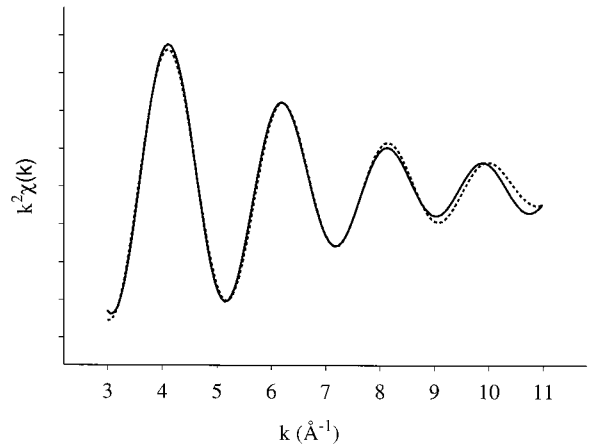

Figure 5. Example of the best fit of the Fourier back-transform of the first coordination peak in Figure 4 for DAB-Am_{32}-$Cu(II)_{16}$. A range of 0.8−2.3 Å was chosen for the back-transform window. Bond distances and coordination numbers for the DAB-Am_n-$Cu(II)_x$ (n = 4 to 64, $x = n/2$) series are listed in Table 2.

Table 2. Bond Distances and Coordination Numbers Obtained from Fitting of the Fourier Back-Transform of the First Coordination Peak in Figure 4 for the DAB-Am_n-$Cu(II)_x$ (n = 4 to 64, $x = n/2$) Series

sample	1 O (Å)[a,b]	3 N (Å)[a,b]
DAB-Am_4-$Cu(II)_2$	1.92	2.02
DAB-Am_8-$Cu(II)_4$	1.95	2.02
DAB-Am_{16}−$Cu(II)_8$	1.96	2.03
DAB-Am_{32}-$Cu(II)_{16}$	1.96	2.04
DAB-Am_{64}-$Cu(II)_{32}$	1.92	2.04

[a] The generally accepted value for the accuracy of Debye−Waller factors and coordination numbers is ±10%; see footnote *c*. [b] The accuracy on distances is taken as ±0.01 Å; see footnote *c*. [c] Teo, B. K. *EXAFS, Basic Principles and Data Analysis*; Inorganic Chemistry Concepts Series; Springer-Verlag: New York, 1986; Vol. 9.

obtained for the other DAB-Am_n-$Cu(II)_x$ complexes, Table 2. The bond distances obtained are typical of Cu−O at 1.92 Å and Cu−N at 2.03 Å.[33,35,43,59,61,64]

The results from this analysis fully support a structure that has the Cu(II) surrounded by three nitrogen atoms in the equatorial plane and an oxygen atom at 1.92 Å at the base of the pyramid. An axial oxygen atom at approximately 2.6 Å completes the square-based pyramid. The oxygen atom in the equatorial plane and the other oxygen atom in the axial position could be associated with the methanol solvent, nitrate anions, or water; we are currently unable to further delineate the structure of the Cu complex. A representation of the Cu(II)-dendrimer end-group structure is shown schematically in Figure 6 for DAB-Am_{16}-$Cu(II)_8$.

Reduction of the DAB-Am_n-$Cu(II)_x$ Complexes and Structural Evaluation of the Resulting Cu(0) Nanocluster-Dendrimer Composites. Samples obtained from reduction of DAB-Am_n-$Cu(II)_x$ (n = 4 to 64, $x = n/2$) with a fixed concentration

(62) All possible combinations for a total of 4 atoms were considered when the fitting procedures were implemented.

(63) The additional peaks in the Fourier transform data are due to contributions arising from multiple scattering from the high number of carbon atoms surrounding the Cu(II) or possibly a weakly bound oxygen from water, methanol, or nitrate. In addition, the back Fourier transform of the peaks between 2 and 4 Å presents some characteristics of heavy element backscattering. Furthermore, a beat node indicative of atoms with very different backscattering function frequencies can be observed in the EXAFS function. Thus, the proximity of another copper atom contributing to the EXAFS of the absorber cannot be excluded and was considered in the fits.

(64) Alagna, L.; Prosperi, T.; Tomlinson, A. A. G.; Vlaic, G. *J. Chem. Soc., Dalton Trans.* **1983**, 645−648.

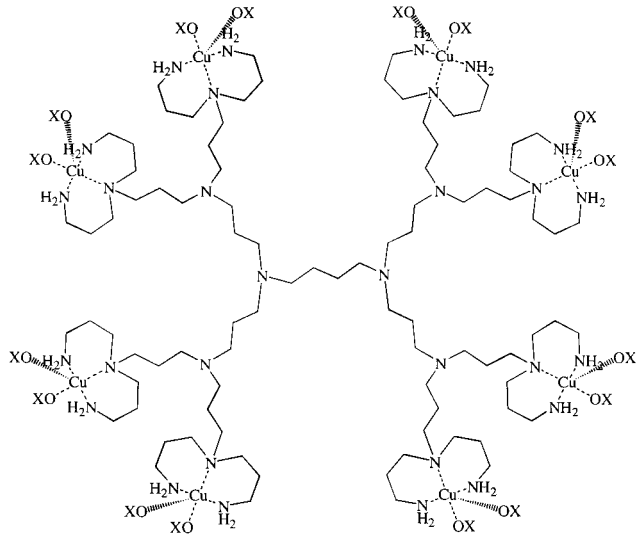

Figure 6. Representation of the DAB-Am^{16}-Cu(II)^{8} complex.

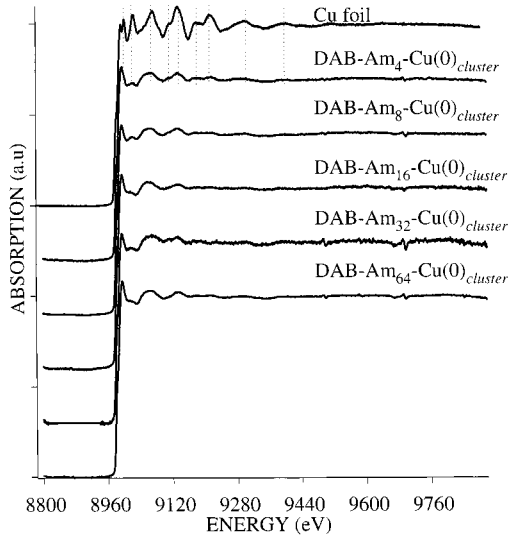

Figure 7. EXAFS spectra of the reduced DAB-Am$_n$-Cu(II)$_x$ (n = 4 to 64, $x = n/2$) complexes and Cu foil.

of Cu(II) have been investigated. The preparation of the reduced materials is summarized here. The requisite amount of a given generation dendrimer solution was added to a MeOH solution containing 2 mM $Cu(NO_3)_2 \cdot 2.5H_2O$ to maintain the primary amine−Cu(II) ratio at 2:1 for all generations (no excess Cu(II) in solution). This procedure results in Cu(II)-dendrimer solutions that contain a fixed concentration of Cu(II) but a varying concentration of dendrimer (1 to 0.0625 mM). Upon reduction of DAB-Am$_n$-Cu(II)$_x$ complexes with methanolic $NaBH_4$, a golden brown solution resulted. UV−vis spectra did not reveal the presence of any remaining DAB-Am$_n$-Cu(II)$_x$, as noted by the lack of the characteristic d−d band for the Cu(II) species at 630 nm[48−50] and Cu(II) signal in the XANES spectra, vide infra. When stored under an inert atmosphere, these solutions were stable (no precipitates or color changes) for a minimum of 3 days, the longest time evaluated. Brown powders were obtained from these solutions by vacuum removal of solvent; the solids were stored and handled under an inert atmosphere at all times.

The EXAFS spectra for powders obtained as described above are displayed and compared to that of a 7.5 μm thick copper foil in Figure 7. The similarities between the spectra of the reduced DAB-Am$_n$-Cu(II)$_x$ complexes and that of the copper foil are striking and demonstrate the existence of metallic

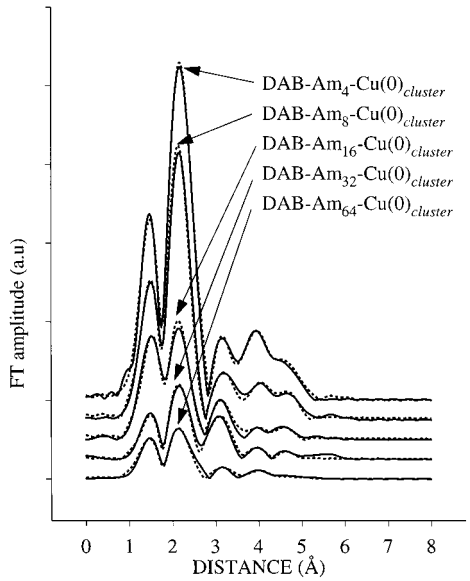

Figure 8. Fourier transforms of the EXAFS function for the reduced DAB-Am$_n$-Cu(II)$_x$ (n = 4 to 64, $x = n/2$) complexes. Experimental data (solid line) and calculated fits (dashed line) are shown. A k range of 3−13 Å^{-1} was used for all of the Fourier transforms so as to eliminate low- and high-k noise contributions.

Cu(0) domains in the reduced DAB-Am$_n$-Cu(II)$_x$, denoted as DAB-Am$_n$-Cu(0)$_{\text{cluster}}$. The position of the K-edge threshold for all of the DAB-Am$_n$- Cu(0)$_{\text{cluster}}$ materials is 1.4 eV higher in energy than that of the pure fcc metal at 8979 eV. This shift in K-edge threshold is characteristic of Cu(0) nanoclusters,[27] thus pointing to their presence in the reduced dendrimer complexes. Furthermore, the amplitudes of the EXAFS features are strongly decreased when compared to those of the fcc copper reference foil, as is expected for Cu(0) nanoclusters.[27] Finally, the presence of nanoclusters is corroborated by UV−vis data. The electronic spectra obtained are characteristic of Cu(0) nanoclusters,[65−69] as noted by the presence of a monotonic increase in the absorbance with increasing energy.[50] Absence of a plasmon band near 550 nm in the UV−vis spectra[50] indicates that the diameter of the nanoclusters is less than 5 nm for all DAB-Am$_n$-Cu-(0)$_{\text{cluster}}$ studied.[65−69]

The Fourier transform of the EXAFS function was obtained for each generation of DAB-Am$_n$-Cu(0)$_{\text{cluster}}$; representative spectra are displayed in Figure 8 for the DAB-Am$_n$-Cu(0)$_{\text{cluster}}$ series. Decreases in the amplitude of the Fourier transforms of the X-ray absorption data as a function of increasing dendrimer generation indicate a decrease in the size of the Cu(0) nanoclusters with increased dendrimer generation, Figure 8. Such a decrease can be correlated to an increase of the surface-to-volume ratio of nanoclusters,[27,70] which points to a decrease in the average Cu(0) nanocluster size with increased size of the dendrimer. Table 3 lists the EXAFS parameters[55] for the successive copper shells of the nanoclusters in the

(65) Rothe, J.; Hormes, J.; Bönnemann, H.; Brijoux, W.; Siepen, K. *J. Am. Chem. Soc.* **1998**, *120*, 6019−6023.
(66) Abe, H.; Charle, K. P.; Tesche, B.; Schulze, W. *Chem. Phys.* **1982**, *68*, 137−141.
(67) Curtis, A. C.; Duff, D. G.; Edwards, P. P.; Jefferson, D. A.; Johnson, B. F. G.; Kirkland, A. I.; Wallace, A. S. *Angew. Chem., Int. Ed. Engl.* **1988**, *27*, 1530−1533.
(68) Lisiecki, I.; Pileni, M. P. *J. Am. Chem. Soc.* **1993**, *115*, 3887−3896.
(69) Lisiecki, I.; Billoudet, F.; Pileni, M. P. *J. Phys. Chem.* **1996**, *100*, 4160−4166.
(70) Traverse, A.; Parent, P.; Mimault, J.; Hagège, S.; Du, J. *Nucl. Instrum. Methods B* **1994**, *84*, 204−207.

Table 3. EXAFS Parameters Obtained from Curve Fitting Analysis for the Reduced DAB-Am_n-Cu(II)$_x$ (n = 4 to 64, $x = n/2$) Complexes and Cu Foil

sample	element coord. shell	coord. no.[a]	bond dist. (Å)[b]	Debye−Waller factor (σ^2)[a]	R
Cu foil	Cu_1	12	2.55	0.0096	6
	Cu_2	6	3.62	0.0147	
	Cu_3	24	4.43	0.0175	
	Cu_4	9	5.02	0.0103	
DAB-Am_4-$Cu(0)_{cluster}$	Cu_1	2.1	2.52	0.0095	10
	Cu_2	1.1	3.54	0.0110	
	Cu_3	2.9	4.41	0.0140	
	Cu_4	1.6	4.96	0.0120	
DAB-Am_8-$Cu(0)_{cluster}$	Cu_1	1.6	2.50	0.0098	8
	Cu_2	0.9	3.51	0.0125	
	Cu_3	1.9	4.42	0.0170	
	Cu_4	1.5	4.96	0.0140	
DAB-Am_{16}-$Cu(0)_{cluster}$	Cu_1	0.8	2.50	0.0110	9
	Cu_2	0.4	3.48	0.0065	
	Cu_3	0.9	4.40	0.0220	
	Cu_4	0.9	4.86	0.0180	
DAB-Am_{32}-$Cu(0)_{cluster}$	Cu_1	0.5	2.50	0.0109	12
	Cu_2	0.3	3.47	0.0040	
	Cu_3	1.2	4.44	0.0200	
	Cu_4	0.5	4.84	0.0140	
DAB-Am_{64}-$Cu(0)_{cluster}$	Cu_1	0.4	2.50	0.0120	12
	Cu_2	0.2	3.51	0.0115	
	Cu_3	0.6	4.47	0.0160	
	Cu_4	0.4	5.00	0.0140	

[a] The generally accepted values for the accuracy of Debye−Waller factors and coordination numbers is ±10%; see footnote *c*. [b] The accuracy on distances is taken as ±0.01 Å; see footnote *c*. [c] Teo, B. K. *EXAFS, Basic Principles and Data Analysis*; Inorganic Chemistry Concepts Series; Springer-Verlag: New York, 1986; Vol. 9.

DAB$_n$-Cu(0)$_{cluster}$ series. The Debye−Waller factors used in the fitting protocol are those determined from previous studies of Cu(0) nanoparticles.[71] Care must be exercised to keep the Debye−Waller factors physically reasonable, or one can obtain improbable coordination numbers. However, the analysis used for the present data was checked in several ways. While the use of other Debye−Waller factors,[29,72] including values for bulk Cu(0), leads to variations in the coordination numbers and absolute sizes of the nanoclusters, *all approaches tested yield a general trend of decreased coordination number, first coordination shell bond distance, and nanocluster size with increased dendrimer generation.*

As has been shown previously, the observed contraction of the first coordination shell Cu−Cu bond distance has been correlated to a decrease in cluster size.[27,28,72] In the work by Montano,[27] Apai,[28] and Gota,[72] it was demonstrated that the size of Cu nanoclusters can be estimated by examination of the first coordination shell Cu−Cu bond distance and the coordination numbers of the successive copper shells.[73] The average Cu−Cu bond distance of the first copper shell obtained for our samples (for example, 2.52 Å for DAB-Am_4-Cu(0)$_{cluster}$) is very close to that of fcc Cu (2.55 Å) and is found to slightly decrease with increasing generation, reaching 2.50 Å for DAB-Am_{64}-Cu(0)$_{cluster}$. By comparing the bond distances of the first coordination shell Cu−Cu bond distance determined in this study with data from Apai et al.,[28] we estimate a diameter of roughly 4 nm for DAB-Am_4-Cu(0)$_{cluster}$, and 1.5 nm for DAB-Am_{64}-Cu(0)$_{cluster}$. In addition, the ratio of the coordination numbers of one copper shell to the others for a given cluster-dendrimer complex agrees well with the corresponding ratio for bulk fcc Cu(0), Table 3.

The low coordination numbers that are reported in Table 3 for the third and fourth Cu coordination shells could be the result of the presence of small defects caused by a film (copper oxide or dendrimer) on the cluster surface. This hypothesis is substantiated by the presence of an additional peak at ~1.6 Å (without phase shift correction) in the Fourier transforms of all the samples. This peak could arise from a layer of copper oxide at the surface,[74] but its position is also consistent with the binding of nitrogen atoms from the dendrimer to the copper atoms of the cluster surface.[75,76] Although it is difficult to differentiate between nitrogen and oxygen solely on their backscattering properties, a Cu_2O oxide layer on the surface of the cluster would generate a peak in the Fourier transform at about 2.3 Å (without phase shift correction),[74] which is not found for any of the DAB-Am_n-Cu(0)$_{cluster}$ materials. Thus, these observations are consistent with the presence of dendrimers adsorbed on the Cu(0) nanocluster surface through nitrogen functionalities.

Transmission electron microscopy (TEM) images obtained for nanoclusters made by reduction of DAB-Am_n-Cu(II)$_x$ (n = 4 to 64, $x = n/2$) complexes are displayed in Figure 9. Electron diffraction patterns were also obtained for each sample (not shown); the diffractograms indicate a predominant fcc structure, thereby corroborating the EXAFS data. The size distributions (based on cluster diameter) for all of the DAB-Am_n-Cu(0)$_{cluster}$ are compiled in Table 4 and demonstrate that the size dispersity of the Cu(0) nanoclusters is quite low. Furthermore, the TEM images demonstrate a *decrease* in size of the nanoclusters with increasing dendrimer generation, as indicated by the EXAFS studies.

The decrease in Cu(0) nanocluster size with increasing dendrimer generation indicates that the size and possibly the location of the nanoclusters with respect to the dendrimer interior is a function of a property associated with the dendrimer and/or the Cu(0) clusters. We address the location of the Cu(0) nanoclusters first. From simple geometric considerations, a *single* dendrimer cannot entirely contain a Cu(0) nanocluster. For example, the DAB-Am_4 (diameter of ~0.8 nm) should not be able to hold the Cu(0) clusters (diameter of 3.7 nm) made from the Cu(II)-DAB-Am_4 precursor. A similar argument can be made for containment of the Cu(0) nanoclusters by the n = 8−32 dendrimers. Only in the case of the n = 64 dendrimer (diameter of roughly 2.4 nm) is it possible to have some degree of encapsulation of the Cu clusters (diameter ~2 nm). Based on this discussion and the previous conclusion that the dendrimers are adsorbed on the surface of the Cu(0) nanoclusters through nitrogen groups, we speculate that the exact nature of the Cu(0) nanocluster-dendrimer interaction—the number of 3° and 1° amine interactions with the cluster surface and the degree of dendrimer distortion resulting from such interactions—during the formation of the Cu(0) nanoclusters is the cause of the observed size dependence of the nanoclusters on dendrimer generation.

(71) Telgheder, F.-W.; Urban, J. *J. Electron. Spectrosc., Relat. Phenom.* **1998**, *95*, 267−279.

(72) Gota, S.; Gautier, M.; Douillard, L.; Thromat, N.; Duraud, J. P.; Le Fèvre, P. *Surf. Sci.* **1995**, *323*, 163−174.

(73) Although these authors have found different results in the determination of the size of clusters ranging from dimers to 40 Å Cu clusters, they showed that there is a strong correlation between bond distance of the first coordination shell and the size of the clusters. Additionally, they agreed on the decrease of the bond distance being a manifestation of the decrease in size of the cluster.

(74) Lamberti, C.; Spoto, G.; Scarano, D.; Paze, C.; Salvalaggio, M.; Bordiga, S.; Zecchina, A.; Turnes; Palomino, G.; D'Acapito, F. *Chem. Phys. Lett.* **1997**, *269*, 500−508.

(75) Wiell, T.; Klepeis, J. E. *Phys. Rev. B* **1998**, *58*, 1655−1664.

(76) Wende, H.; Arvanitis, D.; Tischer, M.; Chauvistre, R.; Henneken, H.; May, F.; Baberschke, K. *Phys. Rev. B* **1996**, *54*, 5920−5926.

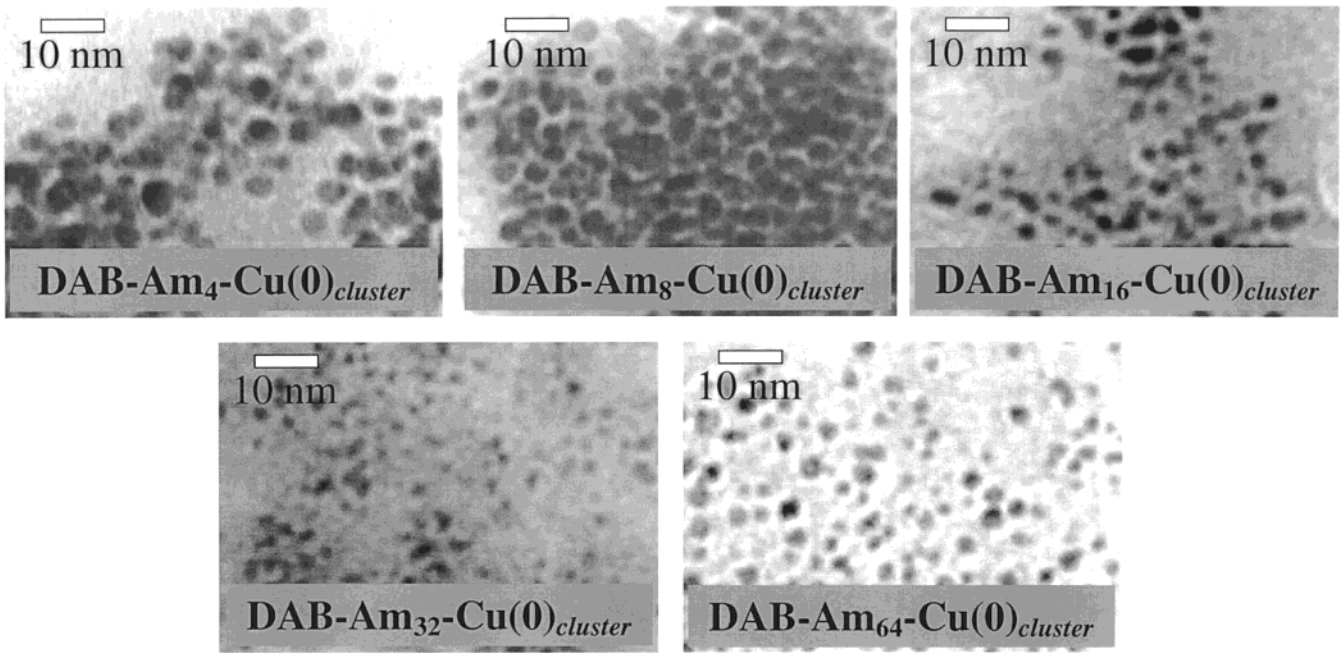

Figure 9. TEM images of copper nanoclusters obtained by reduction of DAB-Am$_n$-Cu(II)$_x$ (n = 4 to 64, $x = n/2$), [Cu(II) = 2 mM].

Table 4. Mean Diameters of Cu Nanoparticles as a Function of Dendrimer Generation[a]

sample	DAB-Am$_4$-Cu(0)$_{cluster}$	DAB-Am$_8$-Cu(0)$_{cluster}$	DAB-Am$_{16}$-Cu(0)$_{cluster}$	DAB-Am$_{32}$-Cu(0)$_{cluster}$	DAB-Am$_{64}$-Cu(0)$_{cluster}$
diameter (nm)[b]	3.71 ± 0.67	3.35 ± 0.63	2.55 ± 0.55	2.29 ± 0.49	1.98 ± 0.50
no. of particles used in calculations	66	51	76	61	256

[a] See Supporting Information for histograms of size distributions. [b] Values are ±1 standard deviation.

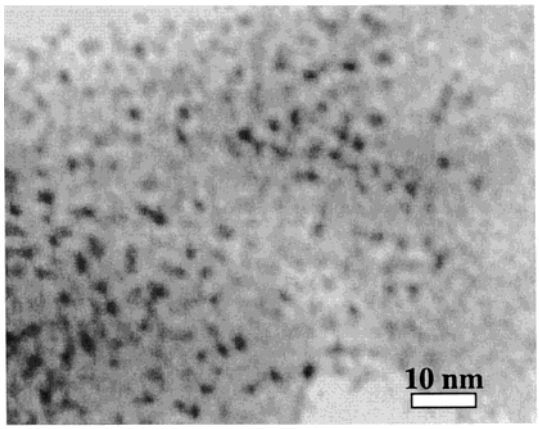

Figure 10. TEM image of the Cu(0) nanoclusters made from DAB-Am$_{64}$-Cu(II)$_{16}$.

Significant decreases in the Cu(0) cluster size and size dispersity can be obtained by varying the ratio of primary amines to Cu(II) ions in the dendrimer precursor. This was achieved through the use of "half-functionalized" materials, such as DAB-Am$_{64}$-Cu(II)$_{16}$, where the ratio of primary amine groups to copper atoms in the nanocluster precursor is increased from 2:1 to 4:1. Upon reduction, *nanoclusters with sizes of 1.60 ± 0.31 nm were obtained*, see Figure 10 and Figure S-6 of the Supporting Information. This result is not due to a mere decrease in the concentration of Cu(II) in the solution, as indicated by TEM data for clusters formed from DAB-Am$_n$-Cu(II)$_x$, $x = n/2$, solutions that were 2-fold lower in total Cu(II)-dendrimer concentration.[50] Further studies aimed at controlling the size of Cu(0) clusters by varying the ratio of amine groups to Cu(II) are underway.

Conclusions

EXAFS and XANES have been successfully applied to the determination of the Cu(II) complex geometry formed upon reaction of $Cu(NO_3)_2 \cdot 2.5\,H_2O$ with poly(propylene imine) dendrimers containing 4 to 64 primary amine groups. These techniques, routinely applied in the study of inorganic materials and catalysts, offer a powerful tool for the structural investigation of supramolecular metal complexes such as the Cu-dendrimer complexes studied in this work. Analysis of the XANES spectra points to an identical environment of the Cu ions in each of the dendrimer end-groups for each generation. The DAB-Am$_n$-Cu(II)$_x$ complexes were found to be pentacoordinate with a square-base pyramidal geometry. Each Cu ion binds to three nitrogens from the dendrimer dipropylene triamine end group (Cu−N distance = 2.03 Å) and an oxygen atom completes the equatorial plane (Cu−O distance = 1.92 Å). Another oxygen atom occupies an axial position at about 2.6 Å. To our knowledge, this is the first study that has given clear geometric information on the complexation of Cu(II) poly(propylene imine) dendrimers; such structural information on the precursor is essential for developing a clear picture of Cu(0) nanocluster formation.

The evidence of nanocluster formation upon reduction with $NaBH_4$ is demonstrated in the XANES data by a shift of the K-edge threshold of 1.4 eV. The EXAFS results indicate a decrease in the size of the clusters with increasing dendrimer generation and are in agreement with the TEM results. However, the presence of a peak at about 1.6 Å in the Fourier transforms of the DAB-Am$_n$-Cu(0)$_{cluster}$ indicates a complex environment of the copper atoms at the cluster surface. We attribute the presence of this peak to Cu−N bonds between the dendrimer and cluster surface as the result of adsorbed dendrimer. On the

basis of this observation and the cluster and dendrimer sizes, we propose a model in which the dendrimer acts as a surfactant for the copper nanoclusters; the nature of dendrimer-cluster interaction evidently leads to the observed size trend. TEM studies demonstrate that it is possible to further decrease the size of the clusters by varying factors such as concentration and the amine to Cu ratio. Future work will focus on the preparation and characterization of smaller monometallic and bimetallic nanoclusters, kinetic studies of the cluster formation process, and the application of EXAFS and XANES to the study of adsorbed Cu-dendrimer complexes on gold surfaces.

Experimental Section

Preparation of DAB-Am$_n$-Cu(II)$_x$ Complexes and DAB-Am$_n$-Cu(0)$_{cluster}$ Nanoparticles. All chemicals were used as received from Aldrich. The DAB-Am$_n$-Cu(II)$_x$ (n = 4, 8, 16, 32, 64; $x = n/2$) complexes were synthesized in the same manner as described by Bosman.[49] To ensure that the proper stoichiometric ratios were obtained (i.e. a given ratio of Cu(II) to dpt end groups), the requisite amounts of methanolic solutions of $Cu(NO_3)_2 \cdot 2.5\ H_2O$ and the corresponding amine-terminated poly(propylene imine) dendrimer with a diaminobutane core (DAB-Am$_n$ (n = 4, 8, 16, 32, 64)) were mixed to result in a final Cu(II) concentration of 2 mM. The faint blue $Cu(NO_3)_2$ solution turned to an intense blue upon mixing with the dendrimer solution. The solution was then stirred for 30 min. Maintaining a Cu(II) concentration of 2 mM throughout the series of dendrimer generations results in the following, in terms of Cu(II)-dendrimer complex concentration: 1 mM DAB-Am$_4$-Cu(II)$_2$, 0.5 mM DAB-Am$_8$-Cu(II)$_4$, 0.25 mM DAB-Am$_{16}$-Cu(II)$_8$, 0.125 mM DAB-Am$_{32}$-Cu(II)$_{16}$, and 0.0625 mM DAB-Am$_{64}$-Cu(II)$_{32}$. Cu nanoparticles were formed by reduction of the DAB-Am$_n$-Cu(II)$_x$ solutions with a 10-fold excess of $NaBH_4$.[77] The reduction resulted in a color change of the solution from blue to golden brown, indicating the formation of nanoclusters, DAB-Am$_n$-Cu(0)$_{cluster}$. TEM images of DAB-Am$_n$-Cu(0)$_{cluster}$ were obtained by placing a drop of the solution on a holey-carbon copper grid, and then immediately transferring the sample into vacuum. The DAB-Am$_n$-Cu(0)$_{cluster}$ samples for EXAFS and XANES were prepared by reduction of the DAB-Am$_n$-Cu(II)$_x$ solutions. As long as these reduced solutions of Cu/dendrimer were kept under inert atmosphere, no precipitate or change of color was observed (over a period of 3 days, the longest time investigated). Powders were obtained by vacuum evaporation of the solvent. The resulting powders were transferred under Ar into an oxygen-free glovebox where they were placed between Kapton tape. The resulting tape/powder samples were kept in an oxygen-free environment for all analyses. The solubility of the brown powders of the DAB-Am$_n$-Cu(0)$_{cluster}$ was not fully investigated. However, these materials do redissolve in methanol and oxidize rather quickly in the presence of oxygen to give greenish/brown solutions.

EXAFS and XANES Measurements. EXAFS and XANES measurements were taken at the Center for Advanced Microstructures and Devices (CAMD) in Baton Rouge, LA. The experiments were performed at the double crystal monochromator (DCM) beamline with a Lemonnier-type monochromator[78] equipped with a pair of Si(400) crystals. The ring was operated at 1.3 or 1.5 GeV with corresponding average ring currents of 140 and 100 mA, respectively. At least two scans were taken for the DAB-Am$_n$-Cu(II)$_x$ (n = 4, 8, 16, 32, and 64, $x = n/2$) from 8779 to 9779 eV in both fluorescence and transmission mode. The powder samples were kept between two pieces of Kapton tape, and no degradation of the samples was observed over time or exposure to radiation. The solution samples were held in a homemade liquid cell with Kapton windows. The fluorescence was measured with a krypton-filled Lytle detector,[79] using a Ni filter and normalized to the incident beam current I_o measured by an ionization chamber placed before the sample. Transmission measurements were taken by monitoring the current in an ionization chamber placed after the sample. Additionally, a copper foil (8979 eV) or copper oxide powder (Cu_2O at 8983.79 eV) was scanned in all measurements for calibration purposes in a third ionization chamber. The calibration was also checked between each sample. The DAB-Am$_n$-Cu(0)$_{cluster}$ (n = 4 to 64) were measured in the transmission mode with Si(311) crystals. Spectra were acquired in the quick-EXAFS mode[80] over the energy range 8800−9900 eV. This instrumentation will be described in detail elsewhere,[81] but is modeled after the apparatus described by Frahm.[80] Briefly, quick-EXAFS entails integrating the motion control with the data acquisition system to facilitate the rapid production of the data sets generated in the course of the typical EXAFS study. The stepper motor stage that drives the monochromator is equipped with an optical encoder that transmits quadrature signals marking angular rotation with a resolution of 1 mdeg. These TTL level signals take the form of pulse trains when the monochromator is rotated. A multifunction data acquisition board that features sampling of analogue and TTL inputs allows instrument readings (represented by scaled analogue voltages) to be correlated with the concurrent position of the rotating monochromator, as determined from the TTL pulse train. Therefore, minimal real-time processing of the sampled encoder and instrumentation signals provide a fast and accurate measurement of photon flux as a function of photon energy.

Data Reduction and Refinements. Data reduction and analysis involving energy calibration, pre-edge and post-edge background subtraction, edge normalization, conversion to k space, and extraction of the EXAFS function χ(k) were carried out by using well-established procedures that adhere to the standards of the International XAFS society.[56,82,83] Winxas 97[84] was used for data analysis in conjunction with autobk[85] and FEFF7.[55]

A range of $k = 3-13$ Å^{-1} was used for the Fourier transforms. The data were available from 0 to 15 Å^{-1} but were truncated to the 3−13 Å^{-1} range so as to eliminate low-k and high-k noise contributions. A range of 0.8−2.3 Å was chosen for the back-transform window. The following expression for $\chi(k)$ was used for the refinements obtained by using the FEFF7 software:[82]

$$\chi(k) = \sum_j N_j S_i(k) F_j(k) e^{-2\sigma_j^2 k^2} e^{-2r_j/\lambda_j(k)} \frac{\sin(2kr_j + \Phi_{ij}(k))}{kr_j^2}$$

The backscattering function $F(k)$, the phase $\Phi(k)$, and the mean free path λ were taken from the generated FEFF files used for the refinements. The distance r, coordination number, and E_0 shift values and Debye−Waller factors were free running parameters. A total of 4 shells was used for Cu (corresponding to the first four coordination shells) in the refinements of the data for the Cu(II)-dendrimer complexes. One additional shell was used in the refinements of the data for the Cu(0) nanoclusters, corresponding to a contribution of Cu−O or Cu−N on the cluster surface. In all cases, the E_0 shift was determined by running a simulation for each shell and was then locked during refinements. Values of the bond distances were first fixed, as were Debye−Waller factors, and then allowed to vary. The number of free parameters in the fitting procedure never exceeded the number of independent parameters ($N_{indp} = 2\Delta k \times \Delta r/\pi$) with no more than 6 parameters allowed to vary at the same time. Multiple scattering paths were not considered during the refinements; this was done so that we could obtain outcomes with meaningful physical significance, and to make a meaningful comparison to EXAFS parameters (bond distances, coordination number, Debye−Waller factors, and residuals) obtained from analysis of a fcc Cu foil sample analyzed in the same manner.

(77) Increasing the molar ratio of $NaBH_4$ does not induce any change in the UV−vis spectra of any of the DAB-Am$_n$-Cu(0)$_{cluster}$ complexes but prevents the rapid oxidation of the copper atoms back to Cu(I) or Cu(II), thus increasing their stability.

(78) Lemonnier, M.; Collet, O.; Depautex, C.; Esteva, J.-M.; Raoux, D. *Nucl. Instrum. Methods* **1978**, *152*, 109−111.

(79) Stern, E. A.; Heald, S. M. *Rev. Sci. Instrum.* **1979**, *50*, 1579−1582.

(80) Frahm, R. *Nucl. Instrum. Methods Phys. Res. Sect. A* **1988**, *270*, 578−581.

(81) Schoonmaker, J. M.; Tittsworth, R. Manuscript in preparation, 2001.

(82) Teo, B. K. *EXAFS: Basic principles and data analysis*; Springer-Verlag: New York, 1986.

(83) Koningsberger, D. C.; Prins, R. *X-ray Absorption−Principles, Applications, Techniques of EXAFS, SEXAFS and XANES*; Wiley and Sons: New York, 1988; Vol. 92.

(84) Ressler, T. *J. Phys. IV* **1997**, *7*, 269−270.

(85) Newville, M.; Caroll, S. A.; O'Day, P. A.; Waychunas, G. A.; Ebert, M. *J. Synchrotron Radiat.* **1999**, *6*, 276−277.

Goodness-of-fit values, referred to as the *R* factor values, for the fit residuals were obtained through Feff 7 refinement using Winxas (as described above), with $R = 100\sum|d_i - t_i|/\sum|d_i|$ (d_i are the experimental data points; t_i are the fit points). A value of $R < 20$ indicates an acceptable fit to the data.

The *k* space refinements were carried out for the Cu(II) species by back Fourier transforming the data to *k* space, followed by a two-shell refinement procedure wherein coordination numbers for both shells were fixed to every possible combination of a total of 4 atoms (3 O, 1 N; 2 O, 2 N; 1 O, 3 N). Multiple scattering paths were not used. Debye−Waller factors were also first fixed, and the distances were constrained between 1.9 and 2.05 Å. Only the *R* values obtained for 3 N and 1 O are indicative of a good fit (10 and 18), also see Table T-1 of the Supporting Information. Additionally, when allowed to float, some parameters obtained from the fitting procedures were unrealistic in value for the cases of 2 O and 2 N, and 3 O and 1 N.

Acknowledgment. The authors wish to acknowledge Roland Tittsworth at the Center for Advanced Microstructures and Devices for assistance with and discussions about the EXAFS experiments. We are also grateful to E. E. Doomes and J. Joubert for help with preliminary studies. We would like to acknowledge Cindy Henk from the Louisiana State University Department of Biology for the TEM images. This work was supported by funding from the National Science Foundation (R.L.M., CHE-9529770 and CHE-0108961; E.D.P., CHE-9616908).

Supporting Information Available: UV−vis spectra of DAB-Am_{32}-$Cu(II)_{16}$ and DAB-Am_{32}-$Cu(0)_{cluster}$ in methanol; TEM images and histograms of clusters produced with 0.2 and 0.1 mM DAB-Am_{16}-$Cu(II)_8$; histograms of clusters in Figures 9 and 10; table of *R* values for various values of N and O atoms used in fits for the Cu(II)-dendrimer data (PDF). This material is available free of charge via the Internet at http://pubs.acs.org.

JA010549D